Photochemical & Photobiological Sciences

Cite this: *Photochem. Photobiol. Sci.*, 2012, **11**, 397

www.rsc.org/pps

PAPER

A quantum chemical investigation of the electronic structure of thionine†

Angela Rodriguez-Serrano,[a] Martha C. Daza,*[a] Markus Doerr*[a,b] and Christel M. Marian[c]

Received 24th August 2011, Accepted 21st October 2011
DOI: 10.1039/c1pp05267e

We have examined the electronic and molecular structure of 3,7-diaminophenothiazin-5-ium dye (thionine) in the electronic ground state and in the lowest excited states. The electronic structure was calculated using a combination of density functional theory and multi-reference configuration interaction (DFT/MRCI). Equilibrium geometries were optimized employing (time-dependent) density functional theory (B3LYP functional) combined with the TZVP basis set. Solvent effects were estimated using the COSMO model and micro-hydration with up to five explicit water molecules. Our calculated electronic energies are in good agreement with experimental data. We find the lowest excited singlet and triplet states at the ground state geometry to be of $\pi\rightarrow\pi^*$ (S_1, S_2, T_1, T_2) and $n\rightarrow\pi^*$ (S_3, T_3) character. This order changes when the molecular structure in the electronically excited states is relaxed. Geometry relaxation has almost no effect on the energy of the S_1 and T_1 states (~0.02 eV). The relaxation effects on the energies of S_2 and T_2 are moderate (0.14–0.20 eV). The very small emission energy results in a very low fluorescence rate. While we were not able to locate the energetic minimum of the S_3 state, we found a non-planar minimum for the T_3 state with an energy which is very close to the energy of the S_1 minimum in the gas phase (0.04 eV above). When hydration effects are taken into account, the $n\rightarrow\pi^*$ states S_3 and T_3 are strongly blueshifted (0.33 and 0.46 eV), while the $\pi\rightarrow\pi^*$ states are only slightly affected (<0.06 eV).

1. Introduction

The 3,7-diaminophenothiazin-5-ium dye, commonly known as thionine, is a cationic photosensitizer which belongs to the phenothiazinium class of compounds. These photosensitizers are an important group of organic compounds which have a variety of applications. Due to its long wavelength light absorption at 590–660 nm, combined with its high efficiency of singlet oxygen production, thionine and its derivatives have been used in many areas such as photodynamic therapy (PDT),[1,2] in the development of biosensors,[3,4] as polymerization photoinitiators,[5,6] in the decontamination of blood products,[7] as nucleic acid probes,[8] and against bacteria,[9–13] viruses and yeasts.[14] Moreover, these compounds are also known to be active against *Plasmodium falciparum* and *Trypanosoma cruzi*.[15,16]

The spectral and photoelectrochemical properties of thionine have been studied extensively in aqueous surfactant solutions,[17] artificial membranes[18] and in the presence of different reducing agents.[19–22]

In dilute aqueous solutions, thionine has a strong absorption at 597 nm (2.08 eV) with a maximum molar absorptivity of 5.52×10^4 dm^3 mol^{-1} cm^{-1},[23] which is found to be redshifted to 603 nm (2.06 eV) in pure ethanol[24] and to 614 nm (2.02 eV) in pyridine.[25] This absorption band has been attributed to the presence of the thionine monomer with a positive resonance charge.[26–28] It is accompanied by a vibrational sideband which appears as a shoulder at ~560 nm and which has been assigned to the $1\leftarrow0$ vibronic transition.[27,28] In addition, a weak absorption band is observed in the ultra-violet region at 281 nm (4.42 eV) (molar absorptivity 4.06×10^4 dm^3 mol^{-1} cm^{-1}) in water,[23] which is also found in ethanolic solutions.[29]

In aqueous solutions, the absorption spectrum of thionine is concentration dependent due to the formation of aggregates in concentrated solution. As the thionine concentration is increased,

[a]*Grupo de Bioquímica Teórica, Universidad Industrial de Santander, Carrera 27, Calle 9, Bucaramanga, Colombia. E-mail: mcdaza@uis.edu.co; Fax: +57 763 23778; Tel: +57 763 23778*
[b]*Facultad de Química Ambiental, Universidad Santo Tomás, Carrera 18 No. 9-27, Bucaramanga, Colombia. E-mail: markusdoerr@gmx.de; Fax: +57 76712677; Tel: +57 76800801*
[c]*Institute of Theoretical and Computational Chemistry, Heinrich Heine University of Düsseldorf, Universitätsstr. 1, D-40225, Düsseldorf, Germany. E-mail: Christel.Marian@uni-duesseldorf.de; Fax: +49 (0)211 8113466; Tel: +49 (0)211 8113209*

† Electronic supplementary information (ESI) available: DFT/MRCI energies of the low-lying states along a linearly-interpolated path between the S_0 and S_1 geometries (Fig. 1); frontier Kohn–Sham BHLYP/TZVP molecular orbitals computed at the T_3 ($n\rightarrow\pi^*$) state minimum (Fig. 2); selected geometrical parameters of the thionine ground state calculated with the B3LYP functional and the TZVP, TZVPP and TZVP+R basis sets (Table 1); vertical singlet and triplet excitation energies ΔE (eV) of thionine calculated using the TZVP+R and the TZVP basis sets (Table 2); DFT/MRCI energies (ΔE), oscillator strengths (f(L)) and dominant contributions (DC) for each of the linearly interpolated geometries between the S_1 and the S_2 minima calculated at the DFT/MRCI/TZVP level (Table 3); geometries and vibrational frequencies of the ground and excited states are provided as molden files: S0.molden, S1.molden, S2.molden, T1.molden, T2.molden and T3.molden. See DOI: 10.1039/c1pp05267e

a second absorption band on the longer-wavelength side of the 597 nm absorption band appears and becomes the major absorption band when the thionine concentration is higher than 10^{-3} M. Below concentrations of 8×10^{-4} M a monomer–dimer model is adequate to describe aqueous solutions of thionine and a dimerization constant of $k_D \approx 4 \times 10^3$ M^{-1} has been determined.[29] Even higher aggregates than dimers are observed at very high concentrations. Additionally, aggregation is also directly related to the chemical nature of the solvent.[28]

In addition to the concentration dependence, the thionine absorption spectrum also shows a marked pH dependence. Depending on the pH, thionine can be found in the following protonation states: neutral thionine (T), monocationic (TH^+) and dicationic thionine (TH_2^{2+}). At pH 2–10, the monocationic thionine (TH^+) is the stable specie, which is only protonated in strongly acidic solutions (pK_a in water is –0.3).[8,30] As the pH decreases below 2, the intensity of the 597 nm absorption band decreases and simultaneously a new absorption band at 673 nm appears.[23] This behaviour has been explained by the protonation of the thionine molecule (TH^+) forming dicationic thionine (TH_2^{2+}), where the proton is located at the heterocyclic (ring-) N atom (N4, see Fig. 1). Neutral thionine (T) has been found in alkaline solutions (pH above 8) and has an maximum absorption wavelength of 520 nm.[31]

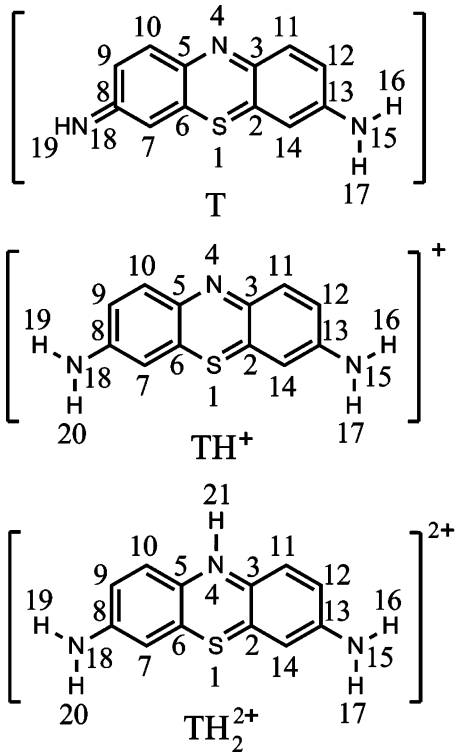

Fig. 1 Chemical structure and atom labeling for thionine.

After excitation with a 532 nm laser pulse (18 ps pulse duration) in 10^{-5} M ethanolic solution, a time-resolved transient spectrum of the singlet excited state of thionine ($^1TH^+$) $S_1 \rightarrow S_n$ can be observed with an absorption maximum at 460 nm and a shoulder around 500 nm. From this spectrum a lifetime of 450 ps was determined for this state,[32] which is close to the value of 360 ps obtained earlier from fluorescence measurements in aqueous solution at pH 2.5.[33] Based on its spectroscopic properties, the first singlet excited state has been described to be essentially of $\pi \rightarrow \pi^*$ character.[34]

Thionine fluoresces with an emission maximum at λ = 610–625 nm whose position does not depend on the nature of the solvent.[35,36] The relative fluorescence yield changes slightly as a function of the solvent. For example, in ethanol the fluorescence yield of thionine is nearly concentration independent ($\varphi_F \approx 0.20$), while it decreases from 0.10 to 0.027 with increasing concentration (2.5×10^{-5} to 2.5×10^{-3} M) in aqueous solutions. This is primarily a result of aggregation because only the monomeric form is weakly fluorescent ($\phi_F = 0.047$ at pH 2.5[34]).[28,37,38]

Upon excitation to a singlet state S_n, thionine can undergo internal conversion to a low-lying singlet state, followed by efficient intersystem crossing ($k_{ISC} = 2.8 \times 10^9$ s^{-1})[39] with a triplet quantum yield $\phi_T = 0.55$ (water, dilute solution, pH 7.2).[40] Two major photochemical pathways are then observed: (a) type I where reducing agents donate an electron to the thionine triplet excited state yielding the semireduced radical, (b) type II where singlet oxygen ($^1O_2$) is generated by energy transfer from the triplet excited state to a ground state oxygen molecule ($^3O_2$) with moderate quantum yield ($\phi_\Delta = 0.58$ in aqueous solutions).[41] It is widely accepted that the major mechanism responsible for the inactivation of bacteria is their reaction with singlet oxygen.

It has been recognized that the triplet state of cationic thionine can be protonated at the ring-N atom in protic solutions forming the acid dicationic triplet form ($^3TH_2^{2+}$).[42] A pK_a value of 7.0 ± 0.1 in methanolic solution and of 6.3 in water has been measured for this equilibrium.[42–44] This means that at pH values close to neutral, the triplet state may exist in protonated and non-protonated forms. These forms can be distinguished by their absorption spectra and have very different lifetimes. The lifetime of the protonated $^3TH_2^{2+}$ form is 7.5 μs, while the non-protonated $^3TH^+$ form has a much longer lifetime of 50 μs. This has consequences for the reactivity of the triplet state.[8] For methylene blue (an amine-methylated derivative of thionine) it has been found that the $^1O_2$ production is approximately five times more efficient in basic than in acidic medium.[45]

Theoretical investigations have proven to be useful to improve the understanding of the photochemistry and photophysics of a variety of systems. Surprisingly, in contrast to the wealth of experimental data which is available for thionine, only a few theoretical studies have been performed on the excited electronic states of this system. In an early computational work, Sommer and Kramer examined the $\pi \rightarrow \pi^*$ electronic excitation energies of thionine employing a semi-empirical configuration interaction (CI) method.[34] More recently Homem-de-Mello *et al.* investigated the electronic spectra of monomeric and dimeric phenothiazinium dyes employing a combination of density functional theory (DFT) and the semi-empirical ZINDO method.[46,47]

In the present computational study we shed more light on the photophysics of thionine. To this end we computed the vertical excitation spectra as well as the electronic structures at the energetic minima of the excited electronic states. In some cases also the potential energy surfaces (PES) between these minima were explored. Because our main results were obtained using isolated thionine, while experimental data is only available for thionine in polar solvents such as water, we also examined the effect of interaction with this solvent. Molecular geometries were obtained employing (time-dependent) density functional theory

(TD-DFT). The electronic structure at these geometries was calculated using the combined density functional theory/configuration interaction method (DFT/MRCI) of Grimme and Waletzke.[48] Our investigation is restricted to monomeric thionine (TH^+) in its monocationic form, which is dominant in dilute solutions.

Our paper is organized as follows: In section 2 we briefly describe the computational methods which were used. In section 3.1 we describe the vertical electronic excitation energies (section 3.1.1) and the adiabatic energies of the excited states of TH^+ (section 3.1.2) in the gas phase. Finally, solvent effects are discussed in section 3.2.

2. Computational details

2.1 Geometry optimization and vibrational frequencies

The geometry of the electronic ground state of TH^+ was optimized at the level of density functional theory (DFT) using the B3LYP functional[49,50] as implemented in the Turbomole 6.1[51] program package. According to our experience this functional yields reliable geometries as long as no charge-transfer states are involved.[52,53] Furthermore, in a recent benchmark it was shown that the B3LYP functional yields reasonable excitation energies comparable to other popular functionals such as PBE0, and somewhat better than long-range corrected functionals such as LC-BLYP and CAM-B3LYP.[54] For the optimization of all electronically excited singlet and triplet states, time-dependent DFT (TD-DFT) was employed.[55] For the ground state as well as for the S_1, T_1 and T_2 electronically excited states, C_{2v} symmetry constraints were employed in the geometry optimization. For the S_2 and T_3 states the geometry optimization ended at saddle points of the PES when C_{2v} symmetry constraints were imposed. Minima could be found when C_s and C_1 symmetry restrictions were applied for the S_2 and T_3 optimizations, respectively.

The optimized structures were proven to be minima on the PES by calculating vibrational frequencies. For the ground state these frequencies were calculated analytically using the aoforce module from the Turbomole package. Frequencies of the excited states were calculated from numerical derivatives of analytic gradients using the NumForce script. Zero-point vibrational energies (ZPVE) were scaled by a factor of 0.9614 as recommended for the B3LYP functional.[56] Geometries and all vibrational frequencies are provided as ESI.†

Three different basis sets were employed: the standard valence triple zeta TZVP and TZVPP basis sets[57] from the Turbomole library, and a TZVP basis set augmented by a set of 1s1p1d diffuse Gaussian Rydberg functions with exponents of 0.01125, 0.009988 and 0.014204 (see ref. 58 for details), which were located at a dummy center in the central ring of the phenothiazinium. The position of this dummy center was allowed to adjust in the geometry optimizations. A numerical grid, usually employed for the cesium atom, was chosen for the quadrature of the exchange correlation at the dummy center. This basis set will be denoted TZVP+R in the following.

2.2 Electronic excitation energies

Vertical electronic excitation energies, transition dipole matrix elements and oscillator strengths were obtained from single point calculations performed at the optimized ground and excited state geometries using the combined density functional theory/multi-reference configuration interaction (DFT/MRCI)[48] method. The DFT/MRCI approach represents an effective means to obtain the electronic spectra for closed-shell organic systems with errors typically less than 0.2 eV.[59]

The main idea of this approach is to include major parts of the dynamic electron correlation by DFT, while static correlation effects are taken into account by short CI expansions. The configuration state functions (CSFs) in the MRCI expansion are built up from Kohn–Sham (KS) orbitals employing the BHLYP functional.[50,60,61] Diagonal elements of the effective DFT/MRCI Hamiltonian are constructed from the corresponding Hartree–Fock based expression and a DFT-specific correction term. All in all the effective DFT/MRCI Hamiltonian contains five empirical parameters which depend only on the multiplicity of the excited state, the number of open shells of a configuration and the density functional employed.

For the ground state geometry as well as for the S_1, T_1 and T_2 excited states, we calculated five roots for each of the four irreducible representations of the C_{2v} point group for both singlet and triplet manifolds. For the S_2 and T_3 excited states, ten and twenty roots for each irreducible representation of the C_s and C_1 point groups were determined.

In addition to these calculations, linearly-interpolated pathways connecting minima of electronically excited states were constructed. Along these pathways the symmetry of the molecule was lowered, and we calculated the same numbers of roots for each irreducible representation as mentioned above.

As is common practice in the DFT/MRCI approach, the CI space was kept moderate by only selecting CSFs whose estimated energy was 1.0 Hartree above the highest reference space energy (selection threshold $\delta E_{sel} = 1.0$). The CI reference space was determined iteratively by first performing a DFT/MRCI calculation with a configuration selection threshold $\delta E_{sel} = 0.8$ and a reference space that included all configurations which can be generated by up to doubly exciting ten electrons within the ten frontier MOs. In the next iteration the selection threshold δE_{sel} was set to 1.0 and all configurations with a squared coefficient of at least 0.003 were included in the reference space. All valence electrons (identified by their MO energies) were correlated.

Fluorescence rates were obtained according to

$$k_F = \frac{4e^2}{3c^3\hbar^4}\left(E_i - E_f\right)^3 \left|\langle f|\hat{r}|i\rangle\right|^2$$

where E_i and E_f are the energies of the excited state (f) and the ground state (i). Expressing k_F in units of s^{-1}, the excited state energies in cm^{-1} and $\langle f|\hat{r}|i\rangle$ *in atomic units* (ea_0) *the numerical prefactor becomes* 2.0261×10^{-6}.

For comparison we also determined the vertical excitation energies using the coupled cluster method with approximate treatment of doubles (CC2) and the TD-DFT method (B3LYP functional), applying the TZVP basis set. The CC2 method[62] is an approximation to the coupled-cluster (CCSD) method where singles equations are retained in the original form and the doubles equations are truncated to the first order in the fluctuating potential. The resolution-of-identity (RI) approximation[63] was used in the calculations employing the CC2 method.

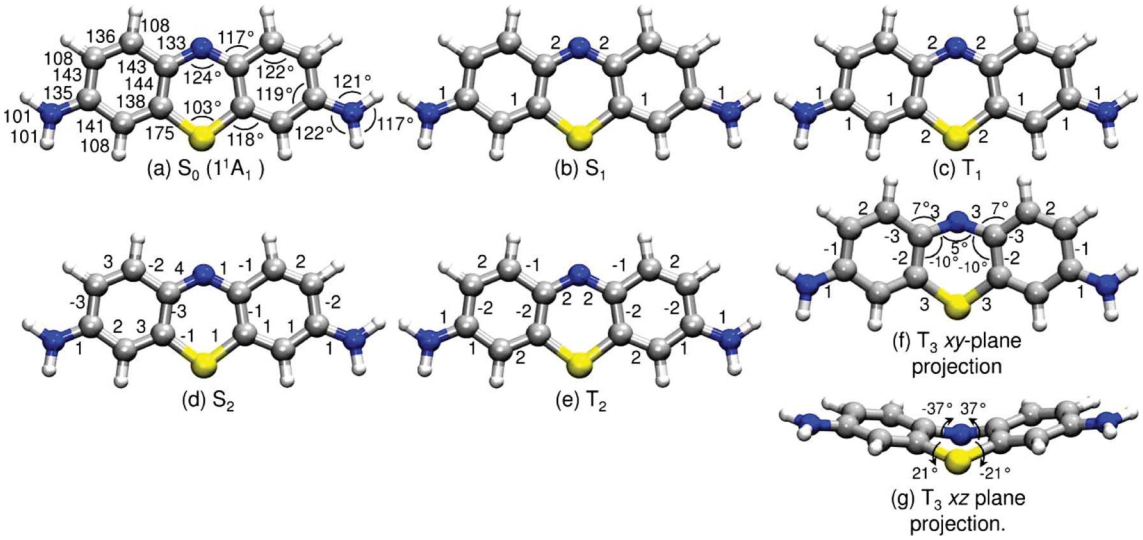

Fig. 2 TD-DFT equilibrium structures of the lowest-lying triplet and singlet excited states of TH^+ in comparison with the ground state geometry. Numbers indicate bond lengths in pm (S_0 structure) and changes of bond lengths relative to the S_0 structure (all other structures). Bond angles and dihedrals are given in degrees. Changes larger than 1 pm and changes >4° are given.

2.3 Solvation model

In order to estimate the spectral shifts due to electrostatic interaction in water, we employed the conductor-like screening model (COSMO)[64,65] which is implemented in the Turbomole package. When the COSMO model was applied, the MRCI expansion was built up from the one-particle basis of COSMO optimized Kohn–Sham orbitals. For the simulation of a bulk water environment we chose a dielectric constant of $\varepsilon = 78$.[66] All calculations involving COSMO were done without symmetry restrictions (C_1 symmetry). For both singlet and triplet multiplicity, 20 roots were computed. In addition the effects of hydrogen bonding in aqueous solution were mimicked by micro-hydration. For this purpose, up to five water molecules were placed near to the heteroatoms of the phenothiazinium ring, the clusters were embedded in a COSMO environment and the ground state of these clusters were optimized without symmetry constraints employing DFT (B3LYP functional) in combination with the TZVP basis set.

3 Results and discussion

3.1 Gas phase: Optimized geometries and electronic spectrum of TH^+

In this section we present the minima of the electronic ground and excited states, as well as the corresponding vertical electronic excitation energies of TH^+.

3.1.1 Ground state minimum and vertical excitation spectrum of TH^+. Selected geometrical parameters of the B3LYP/TZVP ground state equilibrium geometry of TH^+ are presented in Fig. 2(a) and atomic labels are shown in Fig. 1. The ground state minimum of TH^+ is found to be planar and has C_{2v} symmetry. The two C–S bonds have a length of 175 pm and the C–S–C bond angle is 103°. It has been found in a computational study on thiophene that the TZVP basis set is insufficient for a proper description of the C–S bond in this molecule. The results could readily be improved by addition of a second set of polarization functions, while augmentation of the basis set by Rydberg functions had no significant effect on the geometry.[67] In order to test whether in TH^+ the TZVP basis is also insufficient we compared the TZVP geometrical parameters with those calculated with the other two AO basis sets at the ground state geometry, TZVPP and TZVP+R. We found that going beyond the TZVP basis neither affects the C–S bond lengths nor the overall geometry (see Table 1 in ESI†).

To our knowledge, there are no experimental geometrical parameters available for TH^+ which could be used for comparison. Only X-ray data for the amine-methylated derivative, methylene blue, is available in the literature. For methylene blue pentahydrate, the C–S bond lengths are 174 and 172 pm and the C–S–C bond angle is 104°, which is in good agreement with our calculated results for TH^+ obtained with the TZVP basis set.[68]

To test the performance of our approach for describing the excited electronic states, we calculated the vertical excitation energies of TH^+ using three different methods (DFT/MRCI, RI-CC2 and TD-B3LYP) and two different basis sets (TZVP and TZVP+R). The excited-state properties and their leading electronic configurations at the ground state geometry are shown in Table 1, together with theoretical and experimental values from the literature. In addition, the valence molecular orbitals which dominate the corresponding excitations are depicted in Fig. 3. The orbital contributions to the excitations obtained with CC2, DFT/MRCI and TD-B3LYP are very similar. We therefore only show the molecular orbitals which are relevant for the DFT/MRCI results.

Adding diffuse functions to the basis set (TZVP+R) has no significant effect on excitation energies and oscillator strengths. This justifies our choice of the computationally much less demanding TZVP basis set.

At the C_{2v} ground state geometry the DFT/MRCI/TZVP//B3LYP/TZVP calculations predict the lowest singlet excited state S_1 to be a 1^1B_1 state with an excitation energy of 2.29 eV. With an oscillator strength of 0.833 it can be assigned

Table 1 Vertical singlet and triplet excitation energies ΔE (eV) of TH^+

Electronic state	Electronic structure[a]	DFT/MRCI/TZVP//B3LYP/TZVP[b]	DFT/MRCI/TZVP//B3LYP/TZVP (COSMO)[b,c]	TD-B3LYP/TZVP//B3LYP/TZVP[b]	RI-CC2/TZVP//B3LYP/TZVP[b]	Other reported values
$S_0(1^1A_1)$	(0.93) Ground state					
$S_1(1^1B_1)$	(0.80) $\pi_H \rightarrow \pi_L^*$	2.29 (0.833)	2.17 (0.875)	2.74 (0.613)	2.56 (0.836)	2.26[d], 2.08[e], 2.06[f]
$S_2(2^1A_1)$	(0.82) $\pi_{H-1} \rightarrow \pi_L^*$	2.49 (0.012)	2.43 (0.006)	2.73 (0.010)	2.72 (0.009)	
$S_3(1^1B_2)$	(0.79) $n_{H-4} \rightarrow \pi_L^*$	3.11 (0.003)	3.40 (0.018)	3.21 (0.001)	3.51 (0.001)	
$S_4(3^1A_1)$	(0.52) $\pi_{H-2} \rightarrow \pi_L^*$ (0.21) $\pi_H \rightarrow \pi_L^* \pi_H \rightarrow \pi_L^*$	3.56 (0.014)	3.52 (0.003)	4.03 (0.002)[g]	4.33 (0.000)[g]	
⋮	⋮	⋮	⋮	⋮	⋮	
$S_8(4^1A_1)$	(0.64) $\pi_H \rightarrow \pi_{L+1}^*$	4.37 (0.133)	4.25 (0.133)	4.53 (0.089)	4.71 (0.147)	
$S_9(3^1B_1)$	(0.50) $\pi_H \rightarrow \pi_{L+2}^*$ (0.23) $\pi_{H-1} \rightarrow \pi_{L+1}^*$	4.42 (0.056)	4.30 (0.006)	4.62 (0.027)	4.79 (0.163)	
$S_{10}(4^1B_1)$	(0.34) $\pi_{H-1} \rightarrow \pi_L^* \pi_H \rightarrow \pi_L^*$ (0.20) $\pi_{H-1} \rightarrow \pi_{L+1}^*$	4.57 (0.526)	4.46 (0.332)	5.02 (1.058)[h]	5.19 (1.073)[h]	4.42[e]
⋮	⋮	⋮	⋮	⋮	⋮	
$S_{12}(5^1B_1)$	(0.33) $\pi_{H-5} \rightarrow \pi_L^*$ (0.14) $\pi_H \rightarrow \pi_L^* \pi_H \rightarrow \pi_{L+1}^*$ (0.12) $\pi_H \rightarrow \pi_{L+2}^*$	4.90 (0.201)	4.71 (0.369)	5.50 (0.010)[i]	5.73 (–0.002)[i]	
$T_1(1^3B_1)$	(0.92) $\pi_H \rightarrow \pi_L^*$	1.63	1.46	1.53	1.91	
$T_2(1^3A_1)$	(0.88) $\pi_{H-1} \rightarrow \pi_L^*$	2.11	2.07	2.03	2.33	
$T_3(1^3B_2)$	(0.81) $n_{H-4} \rightarrow \pi_L^*$	2.78	3.23	2.61	3.00	
$T_4(2^3A_1)$	(0.78) $\pi_{H-2} \rightarrow \pi_L^*$	3.12	3.06	3.01	3.68	

[a] Dominant contributions at the DFT/MRCI/TZVP level in parentheses. [b] Oscillator strengths (length form) in parentheses. [c] TH^+ 3Wa model, see section 3.2. [d] ZINDO//B3LYP/6-31+G(d) calculation taken from ref. 45. [e] Experimental absorption band taken from ref. 29 and 23, solvent: water. [f] Experimental absorption band taken from ref. 24, solvent: ethanol. [g] The dominant contribution of these states is a combination of two single excitations: $\pi_{H-2} \rightarrow \pi_L^*$ and $\pi_H \rightarrow \pi_{L+1}^*$. [h] The dominant contribution of these states is a combination of two single excitations: $\pi_{H-1} \rightarrow \pi_{L+1}^*$ and $\pi_H \rightarrow \pi_{L+2}^*$. [i] The dominant contribution of these states is a single excitation: $\pi_{H-5} \rightarrow \pi_L^*$, the negative value of the oscillator strength is due to numerical inaccuracies of the RI approximation.

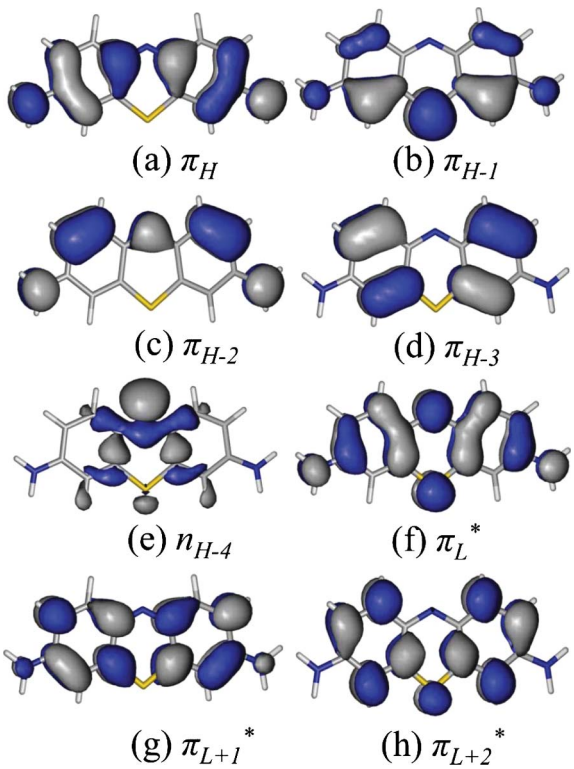

Fig. 3 Frontier BHLYP/TZVP Kohn–Sham molecular orbitals computed at the ground-state (S_0) minimum of TH^+ (isovalue 0.03).

to the strong band maximum in the experimental spectrum. The dominant configuration for this state corresponds to a $\pi_H \rightarrow \pi_L^*$ transition from the HOMO to the LUMO. The occupied π_H HOMO and the virtual π_L LUMO orbitals are of a_2 and b_2 symmetry, respectively. Both contributing MOs are delocalized over the whole molecule.

The second singlet excited state S_2 is a 2^1A_1 $\pi \rightarrow \pi^*$ state dominated by the HOMO-1→LUMO transition. This S_2 state is 0.20 eV higher in energy than S_1 at this geometry. Both π_{H-1} HOMO-1 and the virtual π_L LUMO are of b_2 symmetry, respectively. The following excited state S_3 is 1^1B_2, dominated by a $n_{H-4} \rightarrow \pi_L^*$ (HOMO-4→LUMO) transition. The lone-pair *n*-orbital HOMO-4 (denoted n_{H-4}) is mostly localized at the phenothiazinium nitrogen in the central ring and has a_1 symmetry. The oscillator strength for the S_2 and S_3 transitions of 0.012 and 0.003 indicate negligible absorption intensities.

All three singlet excited states S_1, S_2 and S_3 are dominated by singly excited configurations (weights of 84.4%, 83.2% and 85.1% for states S_1 to S_3). The highest contribution of doubly excited configurations (13.8%) is found for the S_2 state.

The RI-CC2 method predicts the same energetic ordering of the low-lying $\pi \rightarrow \pi^*$ and $n \rightarrow \pi^*$ excited states. Compared to DFT/MRCI, the CC2 excitation energies for the S_1 1^1B_1 ($\pi_H \rightarrow \pi_L^*$), S_2 2^1A_1 ($\pi_{H-1} \rightarrow \pi_L^*$) and S_3 1^1B_2 ($n_{H-4} \rightarrow \pi^*$) states are energetically higher by up to 0.27, 0.30 and 0.40 eV, respectively. These deviations are consistent with recent systematic benchmarks in which CASPT2 reference excitation energies were typically overestimated in CC2 by ~0.3 eV, and underestimated in DFT/MRCI by ~0.2 eV.[59,69] Despite the deviations in excitation energies, the relative energies of the excited states are very similar at the DFT/MRCI and CC2 level. This shows that the different types of the states are well described by these methods.

Table 2 Adiabatic singlet and triplet DFT/MRCI and TD-B3LYP excitation energies ΔE_{adia} (eV) and scaled zero point vibrational corrections (ZPVEC, eV) of the excited states of TH^+ computed using the TZVP basis set. Oscillator strengths for emission at the excited-state minimum are listed in parentheses

Geometry	Electronic structure[a]	DFT/MRCI	TD-B3LYP	ZPVEC[b]
$S_1(1^1B_1)$	(0.80) $\pi_H \rightarrow \pi_L^*$[d]	2.27 (0.790)	2.71 (0.587)	0.02
$S_2(2^1A')$	(0.45) $\pi_{H-1} \rightarrow \pi_L^*$[d]	2.29 (0.269)	2.55 (0.025)	–0.16[c]
	(0.36) $\pi_H \rightarrow \pi_L^*$[d]			
$T_1(1^3B_1)$	(0.92) $\pi_H \rightarrow \pi_L^*$[d]	1.63	1.47	–0.07
$T_2(1^3A_1)$	(0.88) $\pi_{H-1} \rightarrow \pi_L^*$[d]	1.97	1.86	–0.08
$T_3(2^3A)$	(0.50) $n_{H-2} \rightarrow \pi_L^*$[e]	2.31	2.17	0.03
	(0.26) $\pi_{H-4} \rightarrow \pi_L^*$[e]			

[a] Dominant contributions at the DFT/MRCI/TZVP level. [b] Difference between the zero point vibrational energy of the excited state and the zero point vibrational energy of S_0. [c] Does not include the mode with imaginary frequency. [d] MOs are shown in Fig. 3. [e] MOs are shown in Fig. 2 in the ESI.†

The TD-B3LYP/TZVP//B3LYP/TZVP vertical singlet excitation energies are always higher than those calculated with the DFT/MRCI method. In addition, on the TD-B3LYP/TZVP//B3LYP/TZVP PES the bright S_1 1^1B_1 ($\pi_H \rightarrow \pi_L^*$) state is below the S_2 2^1A_1 ($\pi_{H-1} \rightarrow \pi_L^*$) state by 0.01 eV while the energy difference between these two states is 0.16 eV using CC2 and 0.20 eV at the DFT/MRCI level.

No experimental gas phase spectrum is available for comparison. The comparison with aqueous experimental absorption maximum will be postponed to section 3.2, where we discuss the results obtained with our solvation models. Here we only state that the DFT/MRCI gas-phase results are very similar to the previously published ZINDO//B3LYP/6-31+G(d) excitation energy[46] (2.26 eV) and are 0.2 eV larger than the experimental absorption maximum measured in aqueous solutions, which is within the error of the DFT/MRCI method.

Regarding the higher-energy region of the singlet manifold, we found some bright transitions with oscillator strengths larger than 0.1. At the DFT/MRCI/TZVP//B3LYP/TZVP level, transitions to the S_8 (4^1A_1, 4.37 eV), S_{10} (4^1B_1, 4.57 eV) and S_{12} (5^1B_1, 4.90 eV) $\pi \rightarrow \pi^*$ excited states with oscillator strengths of 0.133, 0.532 and 0.201 were obtained. The TD-B3LYP/TZVP method predicts only one optically bright S_{10} (4^1B_1, 5.02 eV) $\pi \rightarrow \pi^*$ state with a strong oscillator strength of 1.058. CC2 predicts three consecutive optically bright transitions to the S_8 4^1A_1 (4.71 eV), S_9 3^1B_1 (4.79 eV) and S_{10} 4^1B_1 (5.19 eV) excited states with oscillator strengths of 0.147, 0.163 and 1.073. The three methods predict the strongest absorption in this energy region as the 4^1B_1 ($\pi \rightarrow \pi^*$) bright state. However, the state character is different at the DFT/MRCI and the TD-DFT and CC2 levels, see Table 2. At the DFT/MRCI level the state has significant contributions from doubly-excited configurations, which cannot be described by TD-DFT and CC2. As a consequence the DFT/MRCI oscillator strength (which is due to the $\pi_{H-1} \rightarrow \pi_{L+1}^*$ singly excited configuration) is lower, resulting in correct relative intensities of the two bright transitions. Furthermore, the calculated DFT/MRCI excitation energy of this state (4.57 eV) is only 0.15 eV higher than the experimental ultraviolet absorption (4.42 eV)[29] measured in aqueous and alcoholic solutions, while the TD-B3LYP and CC2 methods place the absorption at higher energies.

Analogous to the singlet states, in the triplet manifold the lowest-lying excited state T_1 (1^3B_1) is dominated by a $\pi_H \rightarrow \pi_L^*$ HOMO→LUMO transition and has an excitation energy of 1.63 eV computed at the DFT/MRCI/TZVP level. 0.48 eV above this state is the T_2 (1^3A_1) $\pi_{H-1} \rightarrow \pi_L^*$ state with the two electrons residing in the HOMO-1 and LUMO orbitals. At the ground state geometry T_1 and T_2 are located below S_1, T_2 being energetically close to S_1 (0.18 eV). Above T_2 and S_1 is the T_3 state (by 0.67 and 0.49 eV, respectively), characterized by the $n_{H-4} \rightarrow \pi_L^*$ HOMO-4→LUMO transition. All of these triplet states are dominated by single excitations, with weights larger than 90%.

The DFT/MRCI vertical excitation energies of the T_1, T_2 and T_3 states are always higher than those obtained with TD-B3LYP/TZVP (0.10, 0.08 and 0.17 eV, respectively) and lower than the ones obtained with CC2 (0.28, 0.22 and 0.22 eV, respectively). Additionally, at the TD-B3LYP/TZVP level T_3 is 0.15 eV below S_1.

3.1.2 Excited state geometries and adiabatic excitation energies of TH^+. In this section, we discuss the TD-B3LYP minimum energy nuclear arrangements of the two lowest singlet and the three lowest triplet excited states as well as the excitation energies calculated at these geometries. The most important geometrical parameters of the optimized excited states are depicted in Fig. 2. Fig. 4 gives an overview of the energetic locations of the lowest singlet and triplet states at each minimum. The adiabatic excitation energies and the zero point vibrational energy corrections (ZPVEC) are listed in Table 2. The results will be discussed in more detail in the following sections.

S_1 and T_1 minima. We obtained a planar C_{2v} symmetric minimum for the S_1 ($\pi_H \rightarrow \pi_L^*$) excited state, in which the C(5/3)–N(4), C(8/13)–N(18/15) and C(6/2)–C(7/14) bonds are elongated by 2, 1 and 1 pm with respect to their values in the electronic ground state (see Fig. 2(b)). From an energetic point of view the geometry relaxation has almost no effect on the energy of the S_1 ($\pi_H \rightarrow \pi_L^*$) state. Its adiabatic DFT/MRCI excitation energy amounts to 2.27 eV, corresponding to a stabilization of only 0.02 eV. At the same time the electronic ground state is destabilized by 0.07 eV yielding a vertical emission energy of 2.20 eV, which is in good agreement with the maximum of the experimental fluorescence band at 2.04 eV.[35] Due to the small emission energy entering the equation for k_F at the third power, the rate of fluorescence calculated at the S_1 ($\pi_H \rightarrow \pi_L^*$) minimum is rather low ($k_F \approx 1.66 \times 10^8$). This value is in excellent agreement with the experimental one determined at pH 2.5 ($k_F = 1.31 \times 10^8$ s^{-1}).[33]

To shed light on other possible relaxation mechanisms, we constructed a linearly-interpolated path from the Franck–Condon region to the S_1 ($\pi_H \rightarrow \pi_L^*$) minimum (see ESI, Fig. 1†). No crossing

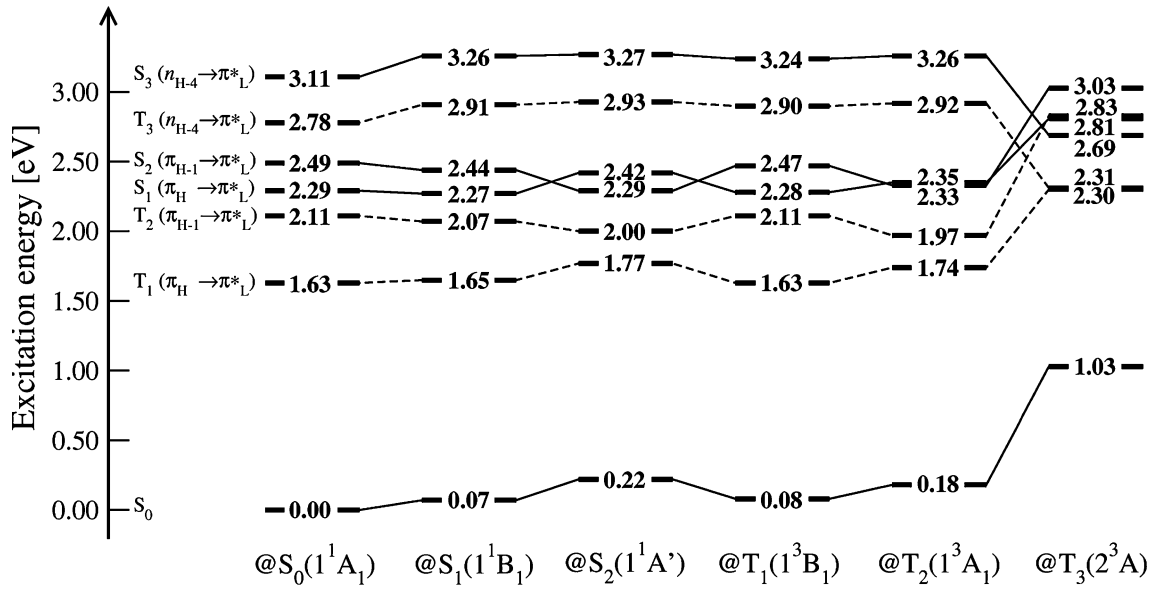

Fig. 4 DFT/MRCI electronic excitation energies [eV] at the various excited state geometries. The electronic ground state energy at the S_0 geometry has been chosen as the common origin.

between electronic states is observed along this path and the dark S_2 ($\pi_{H-1}\rightarrow\pi_L^*$) excited state is always ~0.2 eV above the S_1 state.

As can be expected from the electronic character of these states ($\pi_H\rightarrow\pi_L^*$ transition), the geometry of the T_1 minimum is very similar to that of the S_1 state (see Fig. 2(c)). The main difference between both geometries is the additional widening of the C(2/6)–S(1) and C(7/14)–C(8/13) bonds by 2 and 1 pm, respectively. The adiabatic excitation energy of the T_1 state is 1.63 eV (1.65 eV including the ZPVEC), which is in excellent agreement with the reported values of 1.68 eV[36] and of 1.69 ± 0.07 eV.[34,70,71] As for the S_1 ($\pi_H\rightarrow\pi_L^*$) state, there is almost no energetic relaxation effect on this state.

Furthermore, the excitation energies of the other low-lying singlet and triplet excited states are only slightly affected when proceeding from the Franck–Condon (FC) region to the S_1 and T_1 ($\pi_H\rightarrow\pi_L^*$) minima. It is important to note that the third excited singlet and triplet (S_3 and T_3 $n_{H-4}\rightarrow\pi_L^*$) states are blueshifted between by 0.13 and 0.12 eV at each minimum (S_1 and T_1), moving them energetically away from the S_1 ($\pi_H\rightarrow\pi_L^*$) state, see Fig. 4.

S_2 and T_2 minima. The computed geometry of the stationary point obtained in the optimization of S_2 ($\pi_{H-1}\rightarrow\pi_L^*$) state has C_s symmetry and is characterized by an asymmetric elongation of the bonds. For example, the N(4)–C(5) bond is elongated by 4 pm while the N(4)–C(3) bond by only 1 pm (see Fig. 2(d)). The same holds for the other bond lengths. However, at the level of TD-DFT (TD-B3LYP/TZVP) this structure is found to constitute a saddle point on the PES. One vibrational mode with an imaginary frequency of *i*89.2 cm^{-1} is obtained and corresponds to an out-of-plane movement of the carbon atoms of the central ring and a bending of the amine groups. We calculated the TD-DFT and DFT/MRCI energies along this imaginary normal mode. As has been found before in other systems like flavins,[72] psolaren,[73] cytosine[74] and thiophene,[67] the TD-DFT PES exhibits an extremely shallow double minimum potential well along this imaginary mode, while the DFT/MRCI PES shows a minimum with C_s symmetry.

Furthermore, a distortion along the imaginary normal mode followed by optimization without symmetry constraints (C_1 symmetry) led to a minimum at the TD-B3LYP/TZVP PES, which differs only very slightly from the previously obtained C_s symmetric structure (the difference is a slightly non-planar ring system). At the DFT/MRCI level, this point is energetically higher than the previously described C_s symmetry geometry by 0.01 eV. Therefore we considered the imaginary frequency as an artefact of the TD-DFT (B3LYP) method and chose the C_s symmetric structure as the minimum of the S_2 excited state.

Due to the relaxation effects and the loosening of the symmetry constraints, the irreducible representation of this state changed from A_1 (C_{2v} representation) to A′ (C_s representation). The electronic structure of this S_2 state is now a linear combination of two single excitations $\pi_{H-1}\rightarrow\pi_L^*$ and $\pi_H\rightarrow\pi_L^*$ in *A′* symmetry, with a major contribution from the $\pi_{H-1}\rightarrow\pi_L^*$ transition. In addition, the oscillator strength of this state rises to 0.269 due to mixing with the $\pi_H\rightarrow\pi_L^*$ optically bright transition, see Table 2. At the same time, the S_1 ($\pi_H\rightarrow\pi_L^*$) state corresponds to a linear combination of the $\pi_H\rightarrow\pi_L^*$ and $\pi_{H-1}\rightarrow\pi_L^*$ transitions with a larger contribution of the $\pi_H\rightarrow\pi_L^*$ and is blueshifted by 0.13 eV above the S_2 ($\pi_{H-1}\rightarrow\pi_L^*$) state. This means that during the relaxation from the FC region, an intersection between the S_1 and S_2 PESs occurs.

With regard to the excitation energies, the relaxation effects on S_2 ($\pi_{H-1}\rightarrow\pi_L^*$) are larger than those obtained for the S_1 ($\pi_H\rightarrow\pi_L^*$) state and yield an adiabatic excitation energy of 2.29 eV (a stabilization of 0.20 eV compared with the ground state vertical spectrum), see Table 2 and Fig. 4. The electronic ground state shows a moderate destabilization by 0.22 eV.

In order to investigate the crossing between S_1 and S_2 in more detail, a linearly-interpolated path between the S_1 and the S_2 minima has been constructed. The DFT/MRCI energies of the low-lying states along the path are depicted in Fig. 5. As expected, the two states mix strongly and a crossing of the S_2 and S_1 PESs

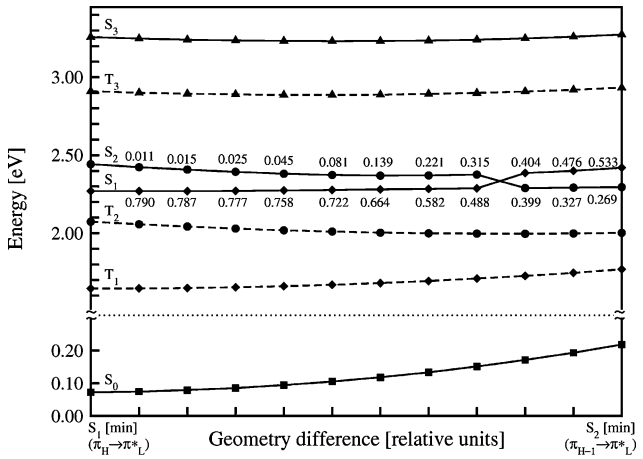

Fig. 5 TH^+ DFT/MRCI energies of the low-lying states along a linearly-interpolated path between the S_1 and S_2 minima. The singlet profiles are represented by solid lines and the triplet profiles by dashed lines.

can easily be reached from the S_1 ($\pi_H \rightarrow \pi_L^*$) minimum in the proximity of the S_2 ($\pi_{H-1} \rightarrow \pi_L^*$) minimum. The mixing of the two states is reflected in the oscillator strengths. At the S_1 ($\pi_H \rightarrow \pi_L^*$) minimum, the S_1 ($\pi_H \rightarrow \pi_L^*$) state has an oscillator strength of 0.790 which is reduced at the crossing region. Even at the S_2 ($\pi_{H-1} \rightarrow \pi_L^*$) minimum, the S_1 ($\pi_H \rightarrow \pi_L^*$) state has significant oscillator strength of 0.533. On the other hand, the oscillator strength of the S_2 ($\pi_{H-1} \rightarrow \pi_L^*$) state increases from 0.010 to 0.339 as the S_1 ($\pi_H \rightarrow \pi_L^*$) geometry gets closer to the crossing region and then drops to 0.269 at the S_2 ($\pi_{H-1} \rightarrow \pi_L^*$) geometry. In the proximity of the S_2 ($\pi_{H-1} \rightarrow \pi_L^*$) minimum the contributions of the $\pi_H \rightarrow \pi_L^*$ and the $\pi_{H-1} \rightarrow \pi_L^*$ configurations, which account for ~80% of the total contributions, are very similar. We therefore expect strong vibronic coupling between these states.

The minimum of the T_2 ($\pi_{H-1} \rightarrow \pi_L^*$) state is C_{2v} symmetric. The C(9)–C(8), C(5)–C(6), C(3)–C(2) and C(12)–C(13) bond lengths are shortened by 2 pm whereas the C(10)–C(5) and C(11)–C(3) bonds by 1 pm (see Fig. 2(e)). At the same time, the N(4)–C(5), N(4)–C(3), C(9)–C(10) and C(11)–C(12) bond lengths are elongated by 2 pm whereas the C(13)–N(15), C(8)–N(14), C(8)–C(7) and C(8)–N(18) bonds are elongated by 1 pm. The adiabatic excitation energy of the T_2 ($\pi_{H-1} \rightarrow \pi_L^*$) state amounts to 1.97 eV, see Table 2. The other singlet and triplet excitation energies calculated at this geometry are slightly higher and the ground state is destabilized by 0.18 eV. It is important to note that the energy gap between the S_1 ($\pi_H \rightarrow \pi_L^*$) and S_2 ($\pi_{H-1} \rightarrow \pi_L^*$) states computed at this geometry is only 0.02 eV, compared with the energy differences between these states at the other minima (0.13–0.20 eV). Nevertheless, the same state ordering is preserved as in the FC region.

S_3 and T_3 minima. The location of minima of the S_3 and T_3 ($n \rightarrow \pi^*$) states was very difficult. Due to mixing of the S_3 state with the lower lying states during optimization it was not possible to find the minimum of the S_3 state and we were only able to locate a minimum of the T_3 state.

In our initial attempts, we started the search for the T_3 minimum using the FC geometry (C_{2v} symmetry) as starting point, which resulted in a planar stationary point on the PES with C_{2v} symmetry. The vibrational analysis indicated that this geometry was a saddle point on the TD-DFT PES with an imaginary frequency of $i45$ cm^{-1}. A scan along this imaginary mode showed that this planar structure was a very flat saddle point on the TD-DFT PES. Distorting this structure along the imaginary mode resulted in a non-planar geometry with C_1 symmetry. Geometry optimization using this structure as the starting point ended at a non-planar stationary point (see Fig. 2(f,g)),which turned out to be a minimum on the PES. Due to the very close proximity of the T_1 ($\pi_H \rightarrow \pi_L^*$) state at this geometry it was necessary to change the default atom displacement from 0.02 a.u. to 0.01 a.u. in the numerical frequency calculation in order to avoid root flipping of the two triplet states.

As can be seen in Fig. 2(g), the geometry of the T_3 excited state is characterized by changes of the C–S–C–C and C–N–C–C dihedral angles of ±21° and ±37° from planarity (180°). Other geometrical changes compared with the ground state geometry include the increase of the C(5)–N(4)–C(3) and C(10/11)–C(5/3)–N(4) angles by 5° and 7°; and the reduction of the C(6/2)–C(5/3)–N(4) angle by 10°. Furthermore, there are elongations of the N(4)–C(5/3) and S(1)–C(6/2) bonds by 3 pm, and a shortening of the C(10)–C(5) and C(3)–C(11) bond lengths by 3 pm.

Geometry relaxation leads to an adiabatic excitation energy of 2.31 eV (see Table 2) corresponding to a stabilization by more than 0.47 eV with respect to the vertical absorption energy (see Table 1). The energetic order of the molecular orbitals changes at this minimum. The energy of the n_{H-4} MO calculated at S_0 is lowered and the MO is now n_{H-2}. Furthermore, a new π_{H-4} MO appears (see ESI, Fig. 2†). Since the V shape of the molecular frame allows for a mixing between n and π character, the electronic wave function of the T_3 state is a linear combination of the $n_{H-2} \rightarrow \pi_L^*$ and $\pi_{H-4} \rightarrow \pi_L^*$ transitions with a larger contribution of the $n_{H-2} \rightarrow \pi_L^*$. Note also that the S_1 ($\pi_H \rightarrow \pi_L^*$) and T_3 ($n \rightarrow \pi^*$) DFT/MRCI adiabatic energies are nearly degenerate, T_3 still being 0.04 eV above the S_1 minimum (0.05 eV including ZPVEC). This energy difference is below the accuracy of our method, so we cannot give a definite answer whether T_3 is accessible from S_1.

At the T_3 ($n \rightarrow \pi^*$) minimum, the electronic ground state is strongly destabilized by 1.03 eV (see Fig. 4). This non-planar nuclear arrangement is very favourable for the $n \rightarrow \pi^*$ electronic states indicated by a reversal of the energetic ordering of the $n \rightarrow \pi^*$ and the $\pi \rightarrow \pi^*$ states with respect to the FC region. At the T_3 minimum the S_3 $n \rightarrow \pi^*$ excited state is below the S_1 $\pi_H \rightarrow \pi_L^*$ state by 0.12 eV and below the S_2 $\pi_{H-1} \rightarrow \pi_L^*$ state by 0.34 eV. The T_3 ($n \rightarrow \pi^*$) excited state is nearly degenerate to the T_1 ($\pi_H \rightarrow \pi_L^*$) state (0.01 eV above) and 0.52 eV below the T_2 ($\pi_{H-1} \rightarrow \pi_L^*$) state at the T_3 ($n \rightarrow \pi^*$) geometry. The change of the energetic order of the states is due to intersections between them, which lie very close to the T_3 ($n \rightarrow \pi^*$) minimum (see Fig. 4 and Fig. 6). Moreover, at this region of the coordinate space the energy of the T_3 ($n \rightarrow \pi^*$) state is 0.50 eV lower than the energy of the S_1 $\pi_H \rightarrow \pi_L^*$ state. This suggests the existence of several conical intersections between the electronically-excited singlet and triplet surfaces near to this point.

It is known experimentally that a part of the singlet population undergoes intersystem crossing to the triplet states. Intersystem crossing is expected to be efficient if the singlet and triplet states involved are close in energy, their spin–orbit coupling is reasonably strong and the density of vibrational levels is high in the accepting state. According to El-Sayed's rule,[75] sizeable spin–orbit coupling is expected between states with $\pi \rightarrow \pi^*$ and states with $n \rightarrow \pi^*$ character, while the spin–orbit coupling between $\pi \rightarrow \pi^*$ states is

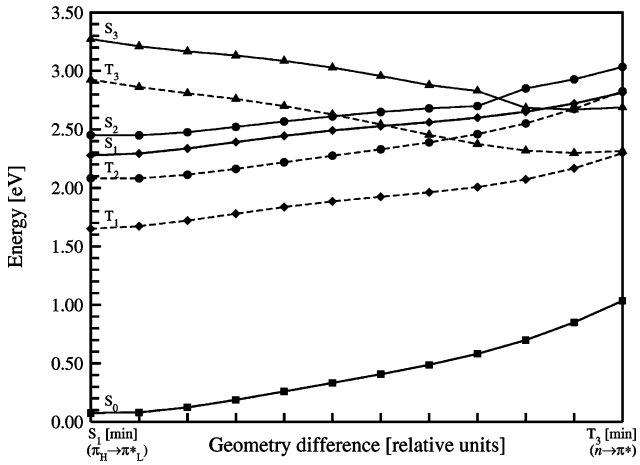

Fig. 6 TH^+ DFT/MRCI energies of the low-lying states along a linearly-interpolated path between the S_1 and T_3 minima. The singlet profiles are represented by solid lines and the triplet profiles by dashed lines.

only weak. Thus, the FC approximation will yield non-efficient intersystem crossing between, *e.g.*, two $\pi\rightarrow\pi^*$ states. In TH^+, the geometry at the T_3 minimum is non-planar, so there is no strict separation between $n\rightarrow\pi^*$ and $\pi\rightarrow\pi^*$ states, (see ESI, Fig. 2(c,e)†). However, even at the non-planar T_3 ($n\rightarrow\pi^*$) minimum, the T_3 state still has predominantly $n\rightarrow\pi^*$ character, so we expect sizeable spin–orbit coupling between T_3 and $\pi\rightarrow\pi^*$ singlet states. According to our results the lowest vibronic level of T_3 ($n\rightarrow\pi^*$) is located slightly above the lowest vibronic level of S_1 ($\pi_H\rightarrow\pi_L^*$). In order to further explore possible ISC channels from S_1 we performed a linearly-interpolated scan of the PES between the S_1 ($\pi_H\rightarrow\pi_L^*$) and T_3 ($n\rightarrow\pi^*$) minima (Fig. 6). Along the interpolated path, T_3 ($n\rightarrow\pi^*$) is lowered in energy by about 0.60 eV while the S_1 ($\pi_H\rightarrow\pi_L^*$) energy rises by 0.54 eV. An intersection between the S_1 and T_3 PESs is found about 0.25 eV above the S_1 ($\pi_H\rightarrow\pi_L^*$) minimum, where intersystem crossing is expected to be efficient (due to the linear interpolation this value is an upper limit for the barrier height). Nevertheless, with such energy barrier zero-point motion alone should be insufficient to couple these states. Instead, we expect the transition to be activated by temperature.

Therefore, from the present results, no mechanism for the efficient intersystem crossing in TH^+ can be derived. Even if we assume that T_3 ($n\rightarrow\pi^*$) can be reached from S_1 ($\pi_H\rightarrow\pi_L^*$) in the gas phase, the situation changes when solvent effects are taken into account, which will be discussed in the following section. Possible explanations for the efficient intersystem crossing include the enhancement of intersystem crossing between two $\pi\rightarrow\pi^*$ states by vibronic spin–orbit coupling.[76] An investigation of these effects is in preparation.

3.2 Solvent effects: Vertical excitation energies and comparison with experiment

Because there is no gas-phase spectroscopic data of TH^+ available, we have to refer to measurements in aqueous and alcoholic solution. These solvents are expected to have a significant effect on the electronic structure, so we calculated the vertical excitation energies of TH^+ using several solvation models. Electrostatic effects of the solvent environment were estimated using the COSMO model with a dielectric constant $\varepsilon = 78$ corresponding to water. This model is labeled TH^+C. In a protic solvent, hydrogen bonds between the solute and the solvent are expected to be important, in particular for $n\rightarrow\pi^*$ states. Therefore we created additional models consisting of the solute and one (TH^+1W) to five (TH^+5W) water molecules, which were additionally embedded in a COSMO environment. The optimized ground state structures of these models are presented in Fig. 7. All models were fully optimized at the B3LYP/TZVP level of theory. The vertical excitation energies and oscillator strengths were calculated using the DFT/MRCI method and are presented in Fig. 8.

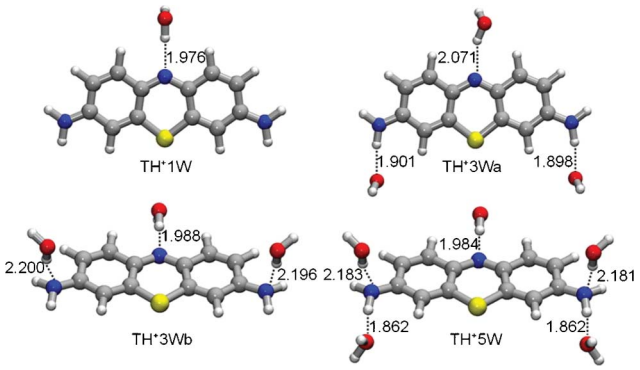

Fig. 7 Ground state minimum of TH^+ hydrogen bonded complexes optimized with COSMO at the B3LYP/TZVP level. Numbers indicate hydrogen bond lengths in Å.

3.2.1 Geometries. Thionine can form hydrogen bonds with water molecules at several sites. The starting geometries were generated by placing water molecules around the thionine molecule in positions where the formation of hydrogen bonds with nitrogen atoms were to be expected: (i) the nitrogen atom of the phenothiazinium central ring (N4 in Fig. 1) can form a hydrogen bond with its lone-pair orbital which is located in the ring plane (H–O–H···N4), (ii) the two amine groups (N15 and N18 in Fig. 1) can form hydrogen bonds with their lone-pair orbitals which are perpendicular to the ring and are involved in the conjugated π-system (H–O–H···N) and (iii) the hydrogen atoms of these two amine groups (N15 and N18 in Fig. 1) can also form hydrogen bonds with water (N–H···O).

The hydrogen bonds between water molecules and the lone pairs of N15 and N18 are relatively weak, indicated by (H–O–H···N) lengths in the range of 2.181–2.200 Å in TH^+3Wb–TH^+5W. The H–O–H···N hydrogen bond formation is accompanied by a slight pyramidization of the amine groups. The hydrogen bonds to nitrogen N4 (H–O–H···N4) of the phenothiazinium central ring and to the hydrogen atoms of the amine groups (N–H···O) are stronger.

3.2.2 Dipole moments and vertical excitation energies. In a simplified picture, the energetic stabilization or destabilization of the ground and excited states in polar solvents is related to their dipole moments and the extent of polarization they induce in the surrounding solvent. Because thionine is charged, its calculated dipole moment depends on the origin of the coordinate system, which is arbitrary. Therefore in Table 3 the differences of the magnitudes of the dipole moments ($\Delta\mu$) calculated relative to the ground state S_0 are listed. According to these results, the effect of

Table 3 Differences of the magnitudes of the dipole moments ($\Delta\mu$, Deybe) of the lowest singlet and triplet electronic states of TH^+ calculated at the DFT/MRCI/TZVP level at S_0. The $\Delta\mu$ magnitudes were calculated relative to the ground state dipole moment

State	S_0	S_1	S_2	S_3	T_1	T_2	T_3
$\Delta\mu$	0.0	0.1	0.4	–0.9	0.1	0.4	–1.1

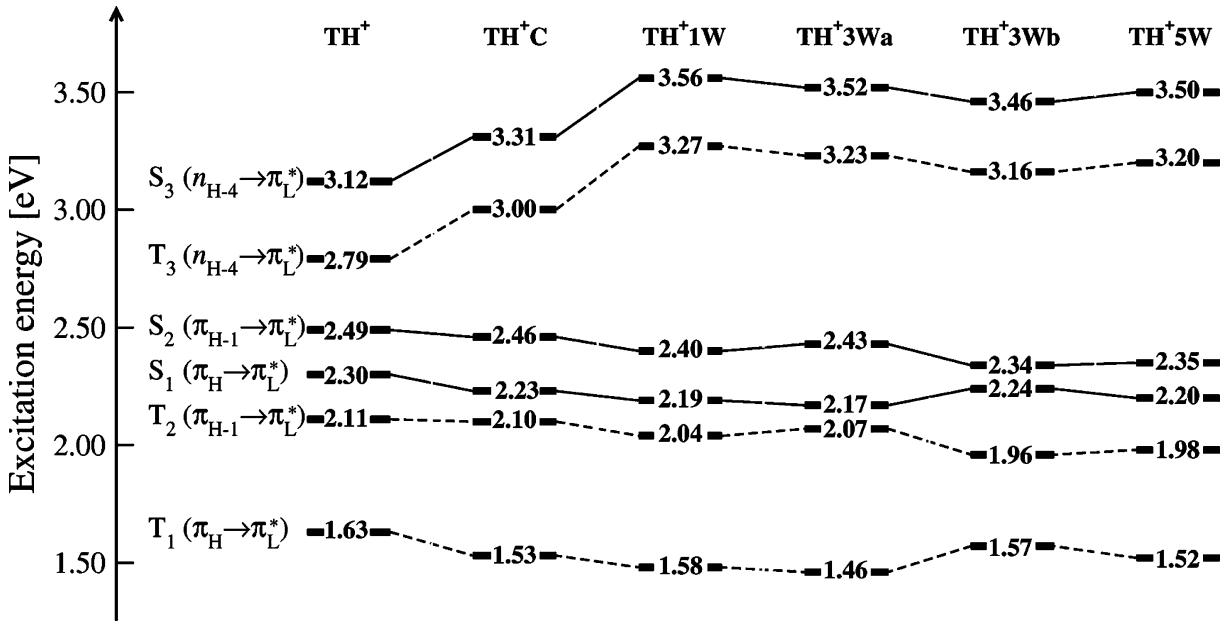

Fig. 8 Comparison of the singlet and triplet vertical excitation energies for the vacuum (TH^+), solvation with COSMO (TH^+C) and micro-hydration with one to five explicit water molecules (TH^+1W–TH^+5W).

a polar solvent on the excitation energies of the S_1–S_2 and T_1–T_2 $\pi\rightarrow\pi^*$ states should be small, while the effect on the S_3 and T_3 $n\rightarrow\pi^*$ states is expected to be stronger.

We first discuss the solvent effect on the energy of the first two lowest excited singlet $\pi\rightarrow\pi^*$ states (see Fig. 8). The effect of the COSMO environment is a slight lowering of the two S_1 and S_2 $\pi\rightarrow\pi^*$ states (0.07 eV for TH^+C), bringing the excitation energy of the bright S_1 state closer to the experimental absorption maximum of 2.07 eV.[32] These solvent shifts are somewhat smaller than the solvent shifts obtained by Homem-de-Mello *et al.*[46] with a polarizable continuum model (–0.29 eV) using a combination of AM1 for optimization of the molecular structure and ZINDO for calculating the electronic spectrum.

The (H–O–H $\cdots$ N4) hydrogen bond (TH^+1W) causes a further redshift of the two $\pi\rightarrow\pi^*$ states which is more pronounced for S_2 than for S_1 due to the different spatial distributions (see Fig. 3) of the contributing orbitals at each state, (HOMO for S_1 and HOMO-1 for S_2). The addition of water molecules at the two amine groups of TH^+ (model TH^+3Wa, N–H $\cdots$ O hydrogen bonds) has no effect on the energies of the two S_1 and S_2 $\pi\rightarrow\pi^*$ states. But if the two water molecules are hydrogen-bonded to the lone-pairs of the two amine groups (model TH^+3Wb, H–O–H $\cdots$ N hydrogen bonds) instead of the amine H-atoms, the energy of S_2 in TH^+3Wb is 0.1 eV lower than with the water molecules in the "equatorial" position (model TH^+3Wa), while the S_1 energy is higher by 0.07 eV. Compared to model TH^+1W, S_1 is slightly blueshifted by 0.05 eV, while S_2 is redshifted by 0.06 eV. Adding two more water molecules (model TH^+5W) partly compensates the effect of the water molecules at the lone-pairs of the two amine groups, see Fig. 8. Assuming that the water molecules preferably bind to the ring-nitrogen N4 and to the H-atoms of the amine groups (an assumption which is supported by the different lengths of the hydrogen bonds), we regard complexes TH^+3Wa and TH^+5W as our best models for solvated TH^+. The absorption energies of the optically bright S_1 $\pi_H\rightarrow\pi_L^*$ state of 2.17 eV (TH^+3Wa) and 2.20 eV (TH^+5W) are in good agreement with the experimental value of 2.07 eV for TH^+.[32]

A significantly larger solvent effect is found for the S_3 $n_{H\text{-}4}\rightarrow\pi_L^*$ state. This state is blueshifted by 0.19 eV by electrostatic effects mimicked by the COSMO environment. The H–O–H $\cdots$ N4 hydrogen bond causes an additional 0.21 eV blueshift. Adding more water molecules partially compensates the blueshift. For our best models, the blueshift of S_3 amounts to 0.33 eV (TH^+3Wa) and 0.28 eV (TH^+5W). The blueshift of the $n\rightarrow\pi^*$ state caused by the H–O–H $\cdots$ N4 hydrogen bond can be qualitatively easily understood: it causes a stabilization of the $n_{H\text{-}4}$ orbital, resulting in a higher excitation energy to the π_L^* orbital, whose energy is only less affected. The triplet states are affected by the solvent environment in a very similar way to their singlet counterparts. The $\pi\rightarrow\pi^*$ states are slightly redshifted, in agreement with previous INDO/CIS calculations in methylene blue–water hydrogen bond complexes,[77] while the $n\rightarrow\pi^*$ states exhibit a strong blueshift.

The strong blueshift of the $n\rightarrow\pi^*$ states in polar and/or protic solvents has consequences for the photophysics of TH^+. In the gas phase, T_3 is nearly degenerate to S_1 and we expect large spin–orbit coupling elements between these states, so $S_1\rightarrow T_3$ is a possible

channel for efficient intersystem crossing. However, in water this channel is no longer accessible due to the strong blueshift of T_3. As discussed above, one possible explanation for efficient intersystem crossing in water is the enhancement of the intersystem crossing rate between two $\pi\rightarrow\pi^*$ states by vibronic spin–orbit coupling.

4. Conclusions

We have examined the molecular and electronic structures of the lowest excited electronic states of monocationic thionine (TH^+) using a combination of (time-dependent) density functional theory and a density functional theory-based multi-reference CI method. We found the lowest two singlet and triplet states to be of $\pi\rightarrow\pi^*$ character, S_1 being the spectroscopically bright state. The third singlet and triplet states both have $n\rightarrow\pi^*$ character. Our estimated fluorescence rate from S_1 is low, in agreement with the experimental value.

Locating the minima of the S_3 and T_3 $n\rightarrow\pi^*$ states turned out to be difficult and we have only been able to locate the minimum of the T_3 state. This minimum has a non-planar structure with an energy which is only 0.04 eV above the adiabatic energy of S_1 $\pi_H\rightarrow\pi_L^*$ minimum. Furthermore, at the T_3 $n\rightarrow\pi^*$ minimum, T_3 is nearly degenerate with T_1 $\pi_H\rightarrow\pi_L^*$, so we expect a conical intersection between T_3 and T_1 very close to the T_3 minimum.

Effects of water solvent were taken into account using the COSMO solvation model and microsolvation with up to five water molecules. The vertical excitation energy calculated with these models is in excellent agreement with the experimental value. The effects of the water environment on the $\pi\rightarrow\pi^*$ states are moderate, but the $n\rightarrow\pi^*$ states are shifted up in energy by several tenths of eV.

Experimentally it is found that TH^+ has a sizeable triplet quantum yield. Qualitatively, according to El-Sayed's rules (see above),[75] we expect sizeable spin–orbit coupling between S_1, which has $\pi\rightarrow\pi^*$ character, and T_3, which has $n\rightarrow\pi^*$ character. However, while T_3 might be accessible from S_1 in the gas phase taking the error bars of our method into account, this is very unlikely in water, where T_3 is shifted up in energy. Therefore with the results presented here we cannot explain the efficient intersystem crossing of TH^+ in water. One possible explanation might be the enhancement of the ISC between two $\pi\rightarrow\pi^*$ states by vibronic coupling. An investigation in this direction is in preparation.

Acknowledgements

We thank Fundación para la Promoción de la Ciencia y la Tecnología del Banco de la República (project 2630) and Universidad Industrial de Santander (project 5169) for financial support. A. Rodriguez-Serrano thanks COLCIENCIAS 'Programa generación bicentenario, becas Francisco José de Caldas'.

References

1 J. P. Tardivo, A. Del Giglio, C. Santos de Oliveira, D. Santesso Gabrielli, H. Couto Junqueira, D. Batista Tadab, D. Severino, R. de Fatima Turchiello and M. S. Baptista, Methylene blue in photodynamic therapy: From basic mechanisms to clinical applications, *Photodiagn. Photodyn. Ther.*, 2005, **2**, 175.
2 D. Gabrielli, E. Belisle, D. Severino, A. J. Kowaltowski and M. S. Baptista, Binding, aggregation and photochemical properties of methylene blue in mitochondrial suspensions, *Photochem. Photobiol.*, 2004, **79**, 227.
3 T. Ohsaka, K. Tanaka and K. Tokuda, Electrocatalysis of poly(thionine)-modified electrodes for oxidation of reduced nicotinamide adenine dinucleotide, *J. Chem. Soc., Chem. Commun.*, 1993, 222.
4 K. Tanaka, S. Ikeda, N. Oyama, K. Tokuda and T. Ohsaka, Preparation of Poly(thionine)-Modified Electrode and Its Application to an Electrochemical Detector for the Flow-Injection Analysis of NADH, *Anal. Sci.*, 1993, **9**, 783.
5 M. G. Neumann and M. R. Rodrigues, The mechanism of the photoinitiation of the polymerization of MMA by the thionine-triethanolamine system, *Polymer*, 1998, **39**, 1657.
6 V. Svoboda, M. J. Cooney, C. Rippolz and B. Y. Liaw, In situ characterization of electrochemical polymerization of methylene green on platinum electrodes, *J. Electrochem. Soc.*, 2007, **154**, D113.
7 M. Wainwright, H. Mohr and W. H. Walker, Phenothiazinium derivatives for pathogen inactivation in blood products, *J. Photochem. Photobiol., B*, 2007, **86**, 45.
8 E. M. Tuite and J. M. Kelly, Photochemical reactions of methylene blue and analogues with DNA and other biological substrates, *J. Photochem. Photobiol., B*, 1993, **21**, 103.
9 M. Wainwright, D. A. Phoenix, J. Marland, D. R. A. Wareing and F. J. Bolton, A study of photobactericidal activity in the phenothiazinium series, *FEMS Immunol. Med. Microbiol.*, 1997, **19**, 75.
10 M. Wainwright, The development of phenothiazinium photosensitisers, *Photodiagn. Photodyn. Ther.*, 2005, **2**, 263.
11 D. A. Phoenix, Z. Sayed, S. Hussain, F. Harris and M. Wainwright, The phototoxicity of phenothiazinium derivatives against Escherichia coli and Staphylococcus aureus, *FEMS Immunol. Med. Microbiol.*, 2003, **39**, 17.
12 M. Wainwright, D. A. Phoenix, S. L. Laycock, D. R. Wareing and P. A. Wright, Photobactericidal activity of phenothiazinium dyes against methicillin-resistant strains of Staphylococcus aureus, *FEMS Microbiol. Lett.*, 1998, **160**, 177.
13 J. W. Foley, X. Song, T. N. Demidova, F. Jalil and M. R. Hamblin, Synthesis and Properties of Benzo[a]phenoxazinium Chalcogen Analogues as Novel Broad-Spectrum Antimicrobial Photosensitizers, *J. Med. Chem.*, 2006, **49**, 5291.
14 M. Wainwright, Photodynamic antimicrobial chemotherapy (PACT), *J. Antimicrob. Chemother.*, 1998, **42**, 13.
15 J. P. Thurston, The chemotherapy of *Plasmodium berghei*. I. Resistance to drugs, *Parasitology*, 1953, **43**, 246.
16 C. Boda, B. Enanga, B. Courtioux, J. C. Breton and B. Bouteille, Trypanocidal activity of methylene blue. Evidence for in vitro efficacy and in vivo failure, *Chemotherapy*, 2006, **52**, 16.
17 B. B. Bhowmik and M. Mukhopadhyay, Photoelectrochemical studies of thionine dye in aqueous surfactant solution, *J. Photochem. Photobiol., A*, 1994, **78**, 173.
18 C. SenVarma and B. B. Bhowmik, Photoinduced interaction of thionine with phospholipid and cholesterol in artificial membranes, *J. Photochem. Photobiol., B*, 1991, **8**, 295.
19 E. Rabinowitch, The photogalvanic effect I: the photochemical properties of the thionine-iron system, *J. Chem. Phys.*, 1940, **8**, 551.
20 E. Rabinowitch, The photogalvanic effect II: the photogalvanic properties of the thionine-iron system, *J. Chem. Phys.*, 1940, **8**, 560.
21 K. G. Mathai and E. Rabinowitch, The thionine-ferrous iron reaction in a heterogeneous system, *J. Phys. Chem.*, 1962, **66**, 663.
22 P. D. Wildes, N. N. Lichtin, M. Z. Hoffman, L. Andrews and H. Linschitz, Anion and solvent effects on the rate of reduction of triplet excited thiazine dyes by ferrous ions, *Photochem. Photobiol.*, 1977, **25**, 21.
23 L. F. Epstein, F. Karush and E. Rabinowitch, A Spectrophotometric Study of Thionine, *J. Opt. Soc. Am.*, 1941, **31**, 77.
24 M. Michaelis, M. P. Schubert and S. Granick, Semiquinone Radicals of the Thiazines, *J. Am. Chem. Soc.*, 1940, **62**, 204.
25 H. Eipper, M. H. Abdel-Kader and H. E. A. Kramer, Thionine triplet relaxation in pyridine: a completely time-resolved forster cycle, *J. Photochem.*, 1985, **28**(3), 433.
26 W. C. Lai, N. S. Dixit and R. A. Mackay, Formation of H Aggregates of Thionine Dye in Water, *J. Phys. Chem.*, 1984, **88**, 5364.
27 G. N. Lewis, O. Goldschmid, T. T. Magel and J. Bigeleisen, Dimeric and Other Forms of Methylene Blue: Absorption and Fluorescence of the Pure Monomer, *J. Am. Chem. Soc.*, 1943, **65**(6), 1150.
28 E. Rabinowitch and L. F. Epstein, Polymerization of Dyestuffs in Solution. Thionine and Methylene Blue, *J. Am. Chem. Soc.*, 1941, **63**, 69.

29 E. G. Kelley and E. G. Miller, Reactions of dyes with cell substances II. The, differential staining of nucleoprotein and mucin by thionine and similar dyes, *J. Biol. Chem.*, 1935, **110**, 119.
30 H. E. A. Kramer and A. Maute, Sensitized photooxygenation according to type i mechanism (radical mechanism) - part I. flash photolysis experiments, *Photochem. Photobiol.*, 1972, **15**, 7.
31 V. E. Nicotra, M. F. Mora, R. A. Iglesias and A. M. Baruzzi, Spectroscopic characterization of thionine species in different media, *Dyes Pigm.*, 2008, **76**(2), 315.
32 B. Patrick and P. V. Kamat, Photosensitization of Large-Bandgap Semiconductors. Charge Injection from Triplet Excited Thionine into ZnO Colloids, *J. Phys. Chem.*, 1992, **96**, 1423.
33 M. D. Archer, M. I. C. Ferreira, G. Porter and C. J. Tredwell, Picosecond study of Stern–Volmer quenching of thionine by ferrous ions, *Nouv. J. Chim.*, 1977, **1**, 9.
34 U. Sommer and H. E. A. Kramer, A theoretical treatment of the electronic states of thionine and related molecules, *Photochem. Photobiol.*, 1971, **13**, 387.
35 M. G. Neumann and M. J. Tiera, The use of basic dyes as photochemical probes, *Química Nova*, 1993, **16**(4), 280.
36 S. Das and P. V. Kamat, Can H-Aggregates Serve as Light-Harvesting Antennae? Triplet–Triplet Energy Transfer between Excited Aggregates and Monomer Thionine in Aersol-OT Solutions, *J. Phys. Chem. B*, 1999, **103**, 209.
37 G. R. Haugen and E. R. Hardwick, Ionic association in aqueous solutions of thionine, *J. Phys. Chem.*, 1963, **67**, 725.
38 G. R. Haugen and E. R. Hardwick, Ionic association in solutions of thionine. II. Fluorescence and solvent effects, *J. Phys. Chem.*, 1965, **69**, 2988.
39 U. Steiner, G. Winter and H. E. A. Kramer, Investigation of physical triplet quenching by electron donors, *J. Phys. Chem.*, 1977, **81**, 1104.
40 M. Nemoto, H. Kokubun and M. Koizumi, Determination of S*-T transition probabilities of some xantene and thiazine dyes on the basis of T-energy transfer. II. Results in the aqueous solution, *Bull. Chem. Soc. Jpn.*, 1969, **42**, 2464.
41 Y. Usui, Determination of quantum yield of singlet oxygen formation by photosensitization, *Chem. Lett.*, 1973, 743.
42 H. Fischer, Light flash investigations on the fading out reaction of thionine with allylthiourea, *Z. Phys. Chem.*, 1964, **43**, 177.
43 E. Vogelmann and H. E. A. Kramer, Photochemical investigations of oxazine, thiazine and selenazine dyes. The reactivity of protolytic triplet forms in electron transfer reactions, *Photochem. Photobiol.*, 1976, **23**, 383.
44 J. Faure, R. Bonneau and J. Joussot-Dubien, Etude en spectroscopie par eclair des colorants thiaziniques en solution aqueuse, *Photochem. Photobiol.*, 1967, **6**, 331.
45 R. Bonneau, R. Pottier, O. Bagno and J. Joussot-Dubien, pH dependence of singlet oxygen production in aqueous solutions using thiazine dyes as photosensitizers, *Photochem. Photobiol.*, 1975, **21**, 159.
46 P. Homem-de-Mello, B. Mennucci, J. Tomasi and A. B. F. da Silva, The effects of solvation in the theoretical spectra of cationic dyes, *Theor. Chem. Acc.*, 2005, **113**, 274.
47 P. Homem-de-Mello, B. Mennucci, J. Tomasi and A. B. F. da Silva, Cationic dye dimers: a theoretical study, *Theor. Chem. Acc.*, 2007, **118**, 315.
48 S. Grimme and M. Waletzke, A combination of Kohn–Sham density functional theory and multi-reference configuration interaction methods, *J. Chem. Phys.*, 1999, **111**, 5645.
49 A. D. Becke, Density-functional thermochemistry. III. The role of exact exchange, *J. Chem. Phys.*, 1993, **98**, 5648.
50 P. A. M. Dirac, Quantum mechanics of many-electron systems, *Proc. R. Soc. London, Ser. A*, 1929, **123**, 714.
51 R. Ahlrichs, M. Bär, H.-P. Baron, R. Bauernschmitt, S. Böcker, N. Crawford, P. Deglmann, M. Ehrig, K. Eichkorn, S. Elliott, F. Furche, F. Haase, M. Häser, C. Hättig, A. Hellweg, H. Horn, C. Huber, U. Huniar, M. Kattannek, A. Köhn, C. Kölmel, M. Kollwitz, K. May, P. Nava, C. Ochsenfeld, H. Öhm, H. Patzelt, D. Rappoport, O. Rubner, A. Schäfer, U. Schneider, M. Sierka, O. Treutler, B. Unterreiner, M. v. Arnim, F. Weigend, P. Weis and H. Weiss, *Turbomole* (vers. 6.1), Universität Karlsruhe, 2009.
52 C. Marian, D. Nolting and R. Weinkauf, The electronic spectrum of protonated adenine: Theory and experiment, *Phys. Chem. Chem. Phys.*, 2005, **7**, 3306.
53 S. Salzmann and C. M. Marian, Effects of protonation and deprotonation on the excitation energies of lumiflavin, *Chem. Phys. Lett.*, 2008, **463**, 400.
54 D. Jacquemin, V. Wathelet, E. A. Perpète and C. Adamo, Extensive TD-DFT Benchmark: Singlet-Excited States of Organic Molecules, *J. Chem. Theory Comput.*, 2009, **5**, 2420.
55 R. Bauernschmitt and R. Ahlrichs, Treatment of Electronic Excitations within the Adiabatic Approximation of Time Dependent Density Functional Theory, *Chem. Phys. Lett.*, 1996, **256**, 454.
56 A. P. Scott and L. Radom, Harmonic vibrational frequencies: an evaluation of Hartree–Fock, Møller–Plesset, quadratic configuration interaction, density functional theory, and semiempirical scale factors, *J. Phys. Chem.*, 1996, **100**, 16502.
57 A. Schäfer, C. Huber and R. Ahlrichs, Fully optimized contracted Gaussian basis sets of triple zeta valence quality for atoms Li to Kr, *J. Chem. Phys.*, 1994, **100**, 5829.
58 C. M. Marian, The guanine tautomer puzzle: quantum chemical investigation of ground and excited states, *J. Phys. Chem. A*, 2007, **111**(8), 1545.
59 M. Schreiber, M. R. Silva-Junior, S. P. A. Sauer and W. Thiel, Benchmarks for electronically excited states: CASPT2, CC2, CCSD and CC3, *J. Chem. Phys.*, 2008, **128**, 134110.
60 C. Lee, W. Yang and R. G. Parr, Development of the Colle-Salvetti correlation-energy formula into a functional of the electron density, *Phys. Rev. B*, 1988, **37**, 785.
61 A. D. Becke, A new mixing of Hartree–Fock and local density-functional theories, *J. Chem. Phys.*, 1993, **98**, 1372.
62 O. Christiansen, H. Koch and P. Jørgensen, The second-order approximate coupled cluster singles and doubles model CC2, *Chem. Phys. Lett.*, 1995, **243**, 409.
63 O. Vahtras, J. Almlöf and M. W. Feyereisen, Integral approximations for LCAO-SCF calculations, *Chem. Phys. Lett.*, 1993, **213**, 514.
64 A. Klamt and G. Schürmann, COSMO: a new approach to dielectric screening in solvents with explicit expressions for the screening energy and its gradient, *J. Chem. Soc., Perkin Trans. 2*, 1993, 799.
65 A. Schäfer, A. Klamt, D. Sattel, J. C. W. Lohrenz and F. Eckert, COSMO Implementation in TURBOMOLE: Extension of an efficient quantum chemical code towards liquid systems, *Phys. Chem. Chem. Phys.*, 2000, **2**, 2187.
66 C. Reichardt, in *Solvents and Solvent Effects in Organic Chemistry*, Wiley-VCH, Weinheim, 1990.
67 S. Salzmann, M. Kleinschmidt, J. Tatchen, R. Weinkauf and C. M. Marian, Excited states of thiophene: ring opening as deactivation mechanism, *Phys. Chem. Chem. Phys.*, 2008, **10**, 380.
68 H. E. Marr and J. M. Stewart, The crystal structure of methylene blue pentahydrate, *Acta Cryst.*, 1973, **B29**, 847.
69 M. R. Silva-Junior, M. Schreiber, S. P. A. Sauer and W. Thiel, Benchmarks for electronically excited states: Time-dependent density functional theory and density functional theory based multireference configuration interaction, *J. Chem. Phys.*, 2008, **129**, 104103.
70 H. E. A. Kramer, M. Hafner and M. Zügel, Bestimmung der Energie des Thionintripletts durch Triplett-Triplett-Energieübertragung, *Z. Phys. Chem.*, 1969, **65**, 276.
71 H. E. A. Kramer, Bestimmung der Energie des Thionintripletts durch Triplett-Triplett-Energieübertragung, *Z. Phys. Chem.*, 1969, **66**, 73.
72 S. Salzmann, J. Tatchen and C. M. Marian, The photophysics of flavins: What makes the difference between gas phase and aqueous solution?, *J. Photochem. Photobiol., A*, 2008, **198**, 221.
73 J. Tatchen and C. M. Marian, Vibronic absorption, fluorescence, and phosphorescence spectra of psoralen: a quantum chemical investigation, *Phys. Chem. Chem. Phys.*, 2006, **8**, 2133.
74 K. Tomić, J. Tatchen and C. M. Marian, Quantum chemical investigation of the electronic spectra of the keto, enol, and keto-imine tautomers of cytosine, *J. Phys. Chem. A*, 2005, **109**, 8410.
75 S. K. Lower and M. A. El-Sayed, The triplet state and molecular electronic processes in organic molecules, *Chem. Rev.*, 1966, **66**, 199.
76 J. Tatchen, N. Gilka and C. M. Marian, Intersystem crossing driven by vibronic spin–orbit coupling: a case study on psoralen, *Phys. Chem. Chem. Phys.*, 2007, **9**, 5209.
77 A. Dias Quintão, K. Coutinho and S. Canuto, Theoretical Study of the Hydrogen Bond Interaction Between Methylene Blue and Water and Possible Role on Energy Transfer for Photodynamics, *Int. J. Quantum Chem.*, 2002, **90**, 634.

